

Determining the Feasibility of Probing the Epoch of Reionization with the 21cm-Ly α Cross-Power Spectrum

Prepared for:

Drs. Daniel Jacobs (Director), Judd Bowman, & Alex Van Engelen

Arizona State University

School of Earth and Space Exploration

Prepared By:

Tyler Cox

Arizona State University

School of Earth and Space Exploration

Astrophysics Senior Thesis

December 5th, 2019

Abstract

The blah blah blah

Contents

I. Contents	ii
II. List of Figures	iii
1 Introduction	1
1.1 The Early Universe	1
1.2 The Epoch of Reionization	2
1.3 Intensity Mapping Experiments	2
1.3.1 The Hydrogen Epoch of Reionization Array	2
1.3.2 SPHEREx: an All-Sky Spectral Survey	2
2. Modeling 21 cm and Lyα Fluctuations	3
2.1. 21 cm Fluctuations	4
2.2. Ly α Fluctuations	5
2.2.1 Galactic	6
2.2.2 Ionized IGM	6
3. Cross-Correlation Studies	8
3.1. Cross-Power Spectrum	8
3.2. Observational Uncertainties	8
3.3. Foreground Contamination	9
4. Conclusions	11
References	13
Appendix	15

List of Figures

1.	Epoch of Reionization Timeline	2
2.	Spin-Flip Transition	2
3.	Resolution and redshift of intensity mapping experiments	3
4.	Layout of HERA	4
5.	SPHEREx	5
6.	Simulated 21cm and Ly α emission	16
7.	21cm Power Spectrum	17
8.	Ly α Power Spectrum	17
9.	Cross-Power Spectrum	18
10.	Cross-Correlation Coefficient	18
11.	Foreground Wedge	19
12.	Noise Power Spectrum	19
13.	Cross Terms Contribution to Noise	20
14.	Cross Power Spec SNR	20

Acknowledgements

First and foremost, I would like to thank the many research advisors who made this work possible, Adam Beardsley, Judd Bowman, Danny Jacobs, and Steven Murray.

I would also like to thank my third committee member, Alex van Engelen.

I would also like to thank my friends and colleagues, who's endless encouragement and blah helped to. In particular, I would like to thank Shane Bechtel, Lily Whitler.

Most importantly, none of this could have been done without the love and support of my family. To my sister, thank you for keeping me humble. To my Mom and Dad, thank you for all you've done.

1 Introduction

1.1 The Early Universe

Immediately following the Big Bang, the Universe was primarily composed of a hot plasma of fundamental particles. In its early state, it was much too hot and dense to form the atoms that form the complex structures the astronomers observe today. Photons that were emitted during this early period scattered off free particles, leaving the Universe opaque to electromagnetic radiation. This lasted until roughly 400,000 years after the Big Bang, at which time the Universe had expanded and cooled sufficiently for electrons to bind to atomic nuclei forming the first atoms of Hydrogen and Helium. Once formed, photons were able to freely propagate through the intergalactic medium (IGM) as cosmic microwave background radiation.

The Cosmic Microwave Background (CMB) is arguably the best studied cosmological period in the history of the universe. Space-based observatories such as WMAP and Planck have measured the CMB with increasing accuracy giving cosmologists insight to the very first fractions of a second after the Big Bang.

Much of the history of the Universe after \sim 1 billion years the Big Bang is observable as well. Optical and infrared observatories such as those done with the Hubble Space Telescope (HST) allows astronomers to regularly observe redshift galaxies out to $z \sim 4$, while a number of objects at $z > 7$ have been observed with gravitational lensing. While some objects have been observed at high redshifts, little is known about the period of cosmological time

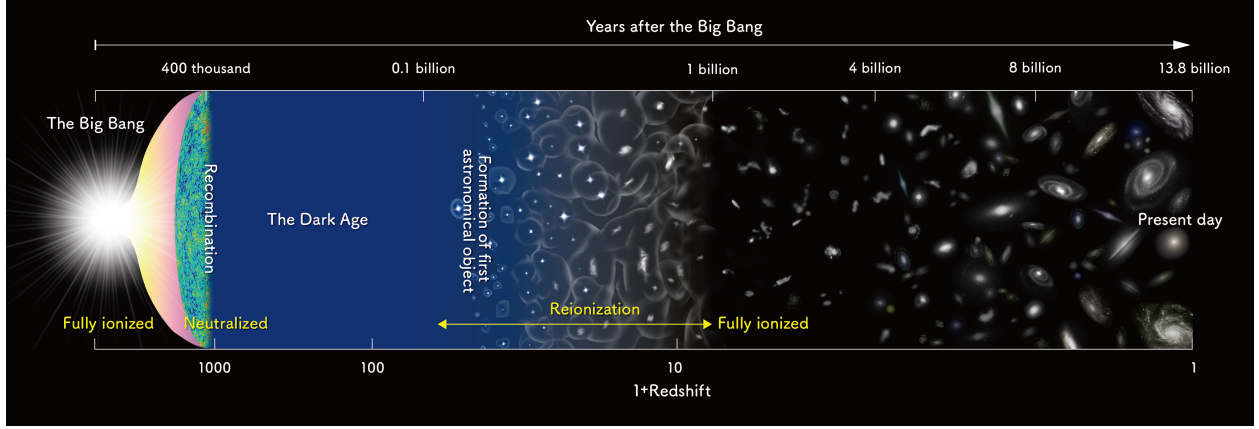


Figure 1. Timeline of the history of the Universe. To the left, is the CMB. To the right, are the stars and galaxies that exist today.

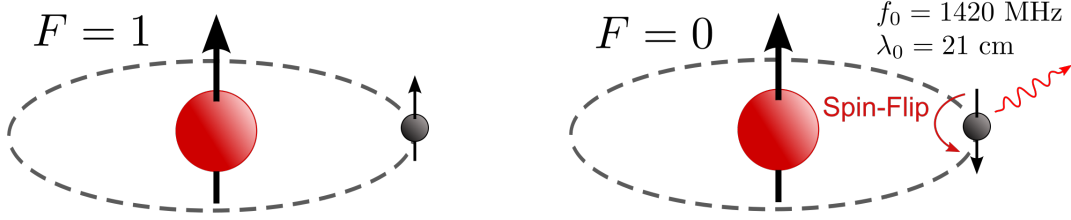


Figure 2. A depiction of the spin flip energy transition of neutral hydrogen. Initially, the spin of the proton and electron are parallel and oriented in the same direction. The energy transition occurs when the electron's spin spontaneously flips from the higher energy parallel alignment to the lower energy anti-parallel alignment, releasing a photon with a wavelength of 21-cm.

between when the.

1.2 The Epoch of Reionization

1.3 Intensity Mapping Experiments

1.3.1 The Hydrogen Epoch of Reionization Array

HERA DeBoer et al. (2017)

1.3.2 SPHEREx: an All-Sky Spectral Survey

SPHEREx looks at things! Doré et al. (2014)

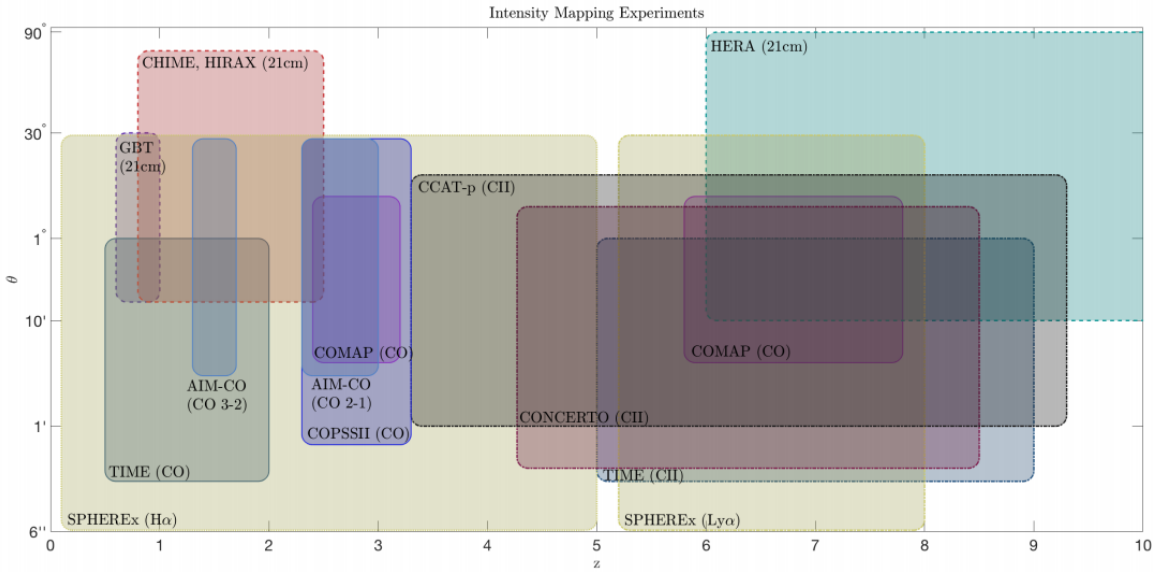


Figure 3

2. Modeling 21 cm and Ly α Fluctuations

In this section, I will discuss the effort to model the 21 cm and Ly α cosmological signals that will be used for cross-correlation later in this work. A significant amount of research has gone into the modeling effort of both 21 cm and Ly α fluctuations during the Epoch of Reionization.

While N-body and radiative transfer codes and analytic models accurately capture the physics of the evolution of galaxies and the IGM at small scales. Semi-numerical simulators on the other hand are much more computationally efficient at modeling the large-scale evolution of the IGM throughout the process of reionization. For this work, I use the semi-numerical simulator of the cosmological 21 cm signal, 21cmFAST [Mesinger et al. \(2011\)](#), to

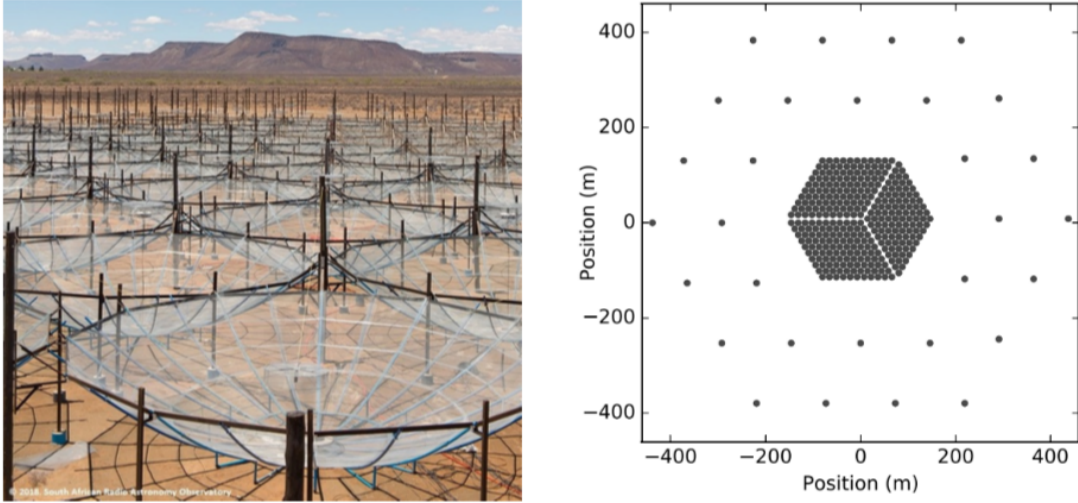


Figure 4. Left: An image of HERA as of late 2017. Right: A map of the full layout of HERA. The final array will be composed of 320 dishes in a tightly packed hexagonal pattern with 30 outriggers for higher resolution. (CITE INSTRUMENT PAPER)

generate the 21 cm signal.

2.1. 21 cm Fluctuations

In the equation above, T_S is the gas spin temperature, T_γ is the CMB temperature, τ_{ν_0} is the optical depth at 21cm frequency, δ_{nl} is the non-linear density contrast $\delta_{\text{nl}} = \rho/\rho - 1$, $H(z)$ is the Hubble parameter, dv_r/dr is the comoving gradient of the line of sight component of the comoving velocity, where all quantities are evaluated at redshift $z = \nu_0/\nu - 1$.

$$\begin{aligned} \delta T_b(z) &= \frac{T_S - T_\gamma}{1+z} \left(1 - e^{-\tau_{\nu_0}}\right) \\ &\approx 27x_{\text{HI}} (1 + \delta_{\text{nl}}) \left(\frac{H}{dv_r/dv + H}\right) \left(1 - \frac{T_\gamma}{T_S}\right) \\ &\quad \times \left(\frac{1+z}{10} \frac{0.15}{\Omega_M h^2}\right)^{1/2} \left(\frac{\Omega_b h^2}{0.023}\right) \text{ mK}, \end{aligned} \quad (1)$$

In the equation above, T_S is the gas spin temperature, T_γ is the CMB temperature, τ_{ν_0} is

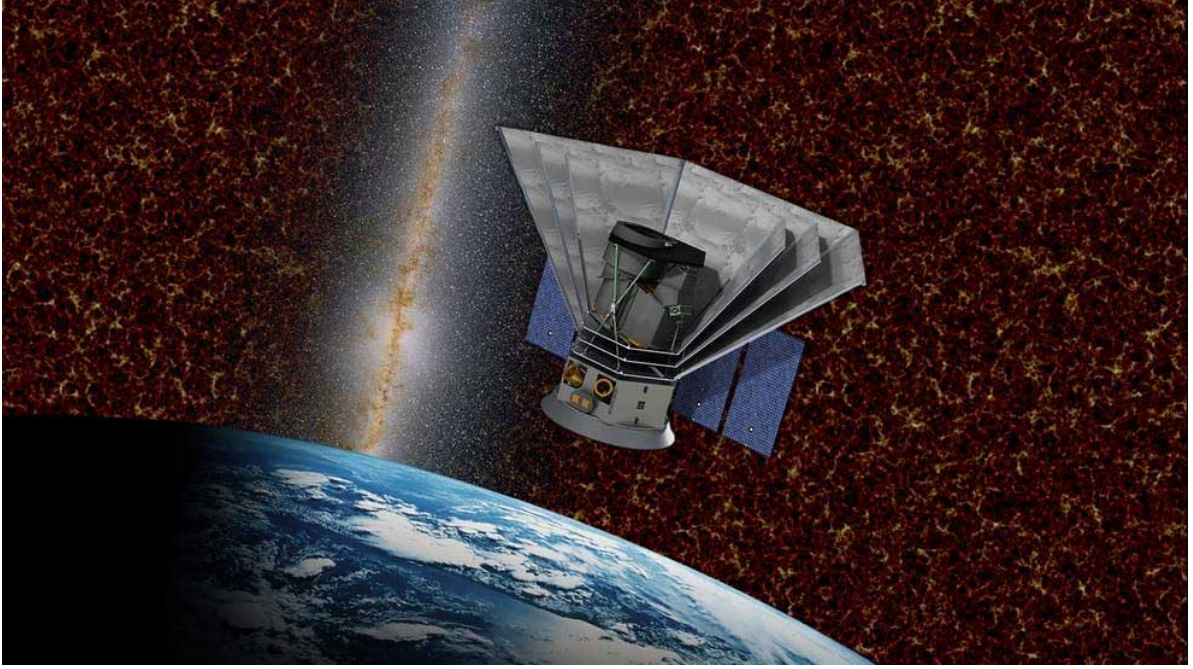


Figure 5. Simulated image of the SPHEREx probe in orbit.

the optical depth at 21cm frequency, δ_{nl} is the non-linear density contrast $\delta_{\text{nl}} = \rho/\bar{\rho} - 1$, $H(z)$ is the Hubble parameter, dv_r/dr is the comoving gradient of the line of sight component of the comoving velocity, where all quantities are evaluated at redshift $z = \nu_0/\nu - 1$.

$$\delta_{21}(\mathbf{x}, z) = \frac{\delta T(\mathbf{x}, z)}{\delta \bar{T}(z)} - 1 \quad (2)$$

where $\delta \bar{T}$ is the spatial average of the 21cm brightness temperature offset $\delta T(\mathbf{x}, z)$. The
her

2.2. Ly α Emission

Here we will describe the parameterization of Ly α emission during reionization. We adopt the technique developed in [Silva et al. \(2013\)](#) and applied in [Heneka et al. \(2017\)](#). While modeling Ly α we focus two locations from which emission happens.

1. *Ly α Emitters:*
2. *Ionized Intergalactic Medium (IGM):*

2.2.1 Galactic

$$L_{\text{rec}}^{\text{gal}}(M, z) = E_{\text{Ly}\alpha} \dot{N}_{\text{Ly}\alpha}(M, z) \quad (3)$$

$$f_{\text{exc}}(M, z) = f_{\text{Ly}\alpha} (1 - f_{\text{esc}}(M, z)) A_{\text{He}} \quad (4)$$

$$L_{\text{exc}}^{\text{gal}}(M, z) = f_{\text{exc}} E_{\text{exc}} \dot{N}_{\text{ion}} \quad (5)$$

$$\text{SFR} = 2.8 \times 10^{-28} \left(\frac{M}{M_{\odot}} \right)^a \left(1 + \frac{M}{c_1} \right)^b \left(1 + \frac{M}{c_2} \right)^d [M_{\odot} \text{ yr}^{-1}] \quad (6)$$

$$I_{\nu}^{\text{gal}}(\mathbf{x}, z) = y(z) d_A^2(z) \frac{L_{\text{rec}}^{\text{gal}}(\mathbf{x}, z)}{4\pi d_L^2} \quad (7)$$

$$\bar{I}_{\nu} = \int_{M_{\min}}^{M_{\max}} dM \frac{dn}{dM} I_{\nu}^{\text{gal}}(M, z) \quad (8)$$

2.2.2 Ionized IGM

Diffuse

$$l_{\text{rec}} = E_{\text{Ly}\alpha} f_{\text{rec}} \dot{n}_{\text{rec}}(\mathbf{x}, z) \quad (9)$$

$$\dot{n}_{\text{rec}}(\mathbf{x}, z) = \alpha_{\text{A}} n_e(z) n_{HII}(z) \quad (10)$$

This is an equation $n_e = x_i(\mathbf{x}, z) n_b(\mathbf{x}, z)$

$$n_b(\mathbf{x}, z) = \bar{n}_{b,0} (1+z)^3 [1 + \delta_{\text{nl}}(\mathbf{x}, z)] \quad (11)$$

$$\alpha_A \approx 4.2 \times 10^{-13} \left(T_K / 10^4 K \right)^{-0.7} (1+z)^3 [\text{cm}^3 \text{ s}^{-1}] \quad (12)$$

$$I_{\text{rec},\nu} = y(z) d_A^2(z) \frac{l_{\text{rec}}(\mathbf{x}, z)}{4\pi d_L^2(z)} \quad (13)$$

Scattered

$$I_\nu = \frac{6E_{\text{Ly}\alpha} d_A^2(z)}{(1+z)^2 d_L^2(z)} J_\alpha(\mathbf{x}, z) \quad (14)$$

$$\delta I_\nu(\mathbf{x}, z) = \sum_i \frac{\nu I_{\nu,i}(\mathbf{x}, z)}{\nu \bar{I}_\nu(z)} - 1 \quad (15)$$

3. Cross-Correlation Studies

3.1. Cross-Power Spectrum

$$\langle \tilde{\delta}(\mathbf{k})\tilde{\delta}(\mathbf{k}') \rangle = (2\pi)^3 \delta_D(\mathbf{k} - \mathbf{k}') P(\mathbf{k}) \quad (16)$$

We can estimate the power spectrum with the relational

$$P(k) \approx \frac{\sum_{\mathbf{k} \in k} \langle |\tilde{\delta}(\mathbf{k})|^2 \rangle}{N_k V} \quad (17)$$

$$\tilde{\Delta}^2(k) = (k) \frac{k^3}{2\pi^2} P(k) \quad (18)$$

$$\Delta^2(k) = (\nu \bar{I}_\nu)^2 \tilde{\Delta}^2(k) \quad (19)$$

S

3.2. Observational Uncertainties

To estimate the feasibility of making a measurement of the 21cm-Ly α cross-power spectrum, it is important to define the sources of error

$$\sigma_{21}(k) = [P_{21}(k) + P_{21,N}(k)] \quad (20)$$

$$P_{21,N} = X^2 Y \frac{T_{\text{sys}}^2}{2t} \frac{\Omega_p^2}{\Omega_{\text{pp}}} \quad (21)$$

Ly α uncertainty

$$\sigma_{\text{Ly}\alpha} = [P_{\text{Ly}\alpha} + P_{\text{Ly}\alpha,\text{N}}] \quad (22)$$

$$P_{\text{Ly}\alpha,\text{N}} = \sigma_{\text{N}}^2 V_{\text{vox}} W_{\text{Ly}\alpha}(k, \mu) \quad (23)$$

$$W_{\text{Ly}\alpha}(k, \mu) = \exp\left(\left(k_{\perp}/k_{\perp,\text{res}}\right)^2 + \left(k_{\parallel}/k_{\parallel,\text{res}}\right)^2\right) \quad (24)$$

$$V_{\text{vox}} = A_{\text{pix}} r_{\text{pix}}$$

21cm-Ly α uncertainty

$$\sigma_{21, \text{Ly}\alpha}^2 = \frac{1}{2} [P_{21, \text{Ly}\alpha}^2 + \sigma_{21} \sigma_{\text{Ly}\alpha}] \quad (25)$$

3.3. Foreground Contamination

$$k_{\parallel} \approx \theta_0 k_{\perp} \frac{D_M(z)}{D_H} \frac{E(z)}{(1+z)} \quad (26)$$

Here is an explanation of the wedge ([Datta et al. \(2010\)](#), [Morales et al. \(2012\)](#))

Cross correlation of cosmological 21cm observations with Ly α intensity mapping surveys have the advantage that 21cm foregrounds do not correlate with the foregrounds. Because the two do not correlate, no power from the foregrounds is added to the cross-power spectrum. However, while the foregrounds don't contribute to the total cross-power spectrum, they do contribute to the overall variance of the measurement, and therefore the errors.

In the previous section, I calculated the cross-power spectrum for the case where foreground are completely uncorrelated (don't contribute to the cross-power spectrum amplitude) and where they did not contribute to the total variance. In this section, I'll take a more realistic and honest approach to calculating the errors by dealing with the 21cm foregrounds in two different ways. There are two primary methods that I chose to deal with

the foregrounds: by relying on the fact that the foregrounds are spectrally smooth and thus confined to an area of the 2D power spectrum known as the wedge and by assuming some imperfect removal method. Each method has advantages and disadvantages.

In addition to avoiding 21cm foregrounds by cutting out k-modes that fall within the wedge, efforts are being made to model 21cm point sources and foregrounds to directly remove them from the data. This technique is known as foreground subtraction. While this modeling foregrounds accurately has been shown to be quite difficult, it gives the added benefit of recovering the foreground modes that fall within the wedge, increasing the signal to noise of the measurement, assuming perfect (or near perfect) foreground subtraction.

While outside the scope of this particular project, foreground subtraction could be a viable method for recovering k-modes afflicted by bright 21cm foregrounds and potentially allow for higher signal to noise measurements of the cross power spectrum, given sufficient enough subtraction.

The total variance on the 21cm-Ly α cross power spectrum measurements would then be written as:

$$\sigma_{21,\text{Ly}\alpha}^2 = \frac{1}{2} [P_{21,\text{Ly}\alpha}^2 + (P_{21} + P_{21,N} + P_{21,F})(P_{\text{Ly}\alpha} + P_{\text{Ly}\alpha,N})] \quad (27)$$

4. Conclusions

Despite the efforts of first-generation 21-cm experiments, the Epoch of Reionization remains one of the most mysterious periods in the universe’s history. Next-generation intensity mapping experiments, such as HERA and SPHEREx, look to shed light on this largely unexplored period. While each instrument should allow for an in-depth study of reionization, synergies between instruments like these will offer independent confirmation on reionization era physics and provide insight on the evolution of the first luminous sources.

While this was a decent proof of concept, a number of potential avenues have the opportunity to be explored in future work. This section BLAH, we provided a treatment of 21-cm foregrounds in which, we avoided the foreground dominated region in cylindrically averaged power spectrum by removing all modes within the foreground wedge. In the future, it might be interesting to explore other methods of foreground removal such as foreground subtraction. While it is likely that even optimistic levels of foreground modeling and subtraction (99.9% NICOLE’S PAPER), would dominate the error budget of the cross-power spectrum, the relatively low noise contribution from SPHEREx may allow the cross-power spectrum to be detectable even in cases of imperfect foreground removal. In addition to an enhanced 21-cm foreground treatment, we ignored infrared foreground removal (CITE PIXEL MASKING SPHEREx PAPER). This likely will not significantly change the amplitude of the cross-power spectrum but could be added for completeness.

In spite of the fact that the cross-power spectrum turnover will remain undetectable by HERA and SPHEREx measurements, given the observational parameters that were chosen, this detection may still allow for constraints on cosmological and astrophysical parameters. In future work, we would like to quantify the accuracy with which the 21cm-Ly α cross-power spectrum can allow us to estimate cosmological parameters. This analysis has been done

with the

In addition to Ly α , 21-cm measurements made by HERA will prove to be complementary to intensity mapping measurements of other spectral lines. In particular, instruments measuring the CO(2-1) rotational line (COMAP) and the CII fine structure line (TIME, CCAT-p, and CONCERTO) will be prime candidates for cross-correlation with HERA in the near future. One possible extension of this work could be to model intensity mapping from these lines during the EoR using 21cmFAST cubes and estimate the feasibility of cross-correlating with these experiments. If the 21cm-CO or 21cm-CII cross-power spectrum proves to be measurable, they should each provide additional confirmation of an EoR detection and give insight into ionized bubble size and mean ionization fraction.

References

- Barry, N., Wilensky, M., Trott, C. M., et al. 2019, ApJ, 884, 1, doi: [10.3847/1538-4357/ab40a8](https://doi.org/10.3847/1538-4357/ab40a8)
- Chang, T. C., Gong, Y., Santos, M., et al. 2015, in Advancing Astrophysics with the Square Kilometre Array (AASKA14), 4
- Datta, A., Bowman, J. D., & Carilli, C. L. 2010, ApJ, 724, 526, doi: [10.1088/0004-637X/724/1/526](https://doi.org/10.1088/0004-637X/724/1/526)
- DeBoer, D. R., Parsons, A. R., Aguirre, J. E., et al. 2017, PASP, 129, 045001, doi: [10.1088/1538-3873/129/974/045001](https://doi.org/10.1088/1538-3873/129/974/045001)
- Doré, O., Bock, J., Ashby, M., et al. 2014, arXiv e-prints, arXiv:1412.4872. <https://arxiv.org/abs/1412.4872>
- Feng, C., Cooray, A., & Keating, B. 2017, ApJ, 846, 21, doi: [10.3847/1538-4357/aa7ff1](https://doi.org/10.3847/1538-4357/aa7ff1)
- Furlanetto, S. R., & Lidz, A. 2007, ApJ, 660, 1030, doi: [10.1086/513009](https://doi.org/10.1086/513009)
- Gong, Y., Silva, M., Cooray, A., & Santos, M. G. 2014, ApJ, 785, 72, doi: [10.1088/0004-637X/785/1/72](https://doi.org/10.1088/0004-637X/785/1/72)
- Heneka, C., Cooray, A., & Feng, C. 2017, ApJ, 848, 52, doi: [10.3847/1538-4357/aa8eed](https://doi.org/10.3847/1538-4357/aa8eed)
- Hutter, A., Dayal, P., Müller, V., & Trott, C. M. 2017, ApJ, 836, 176, doi: [10.3847/1538-4357/836/2/176](https://doi.org/10.3847/1538-4357/836/2/176)
- Hutter, A., Dayal, P., Partl, A. M., & Müller, V. 2014, MNRAS, 441, 2861, doi: [10.1093/mnras/stu791](https://doi.org/10.1093/mnras/stu791)
- Kubota, K., Inoue, A. K., Hasegawa, K., & Takahashi, K. 2019, arXiv e-prints, arXiv:1910.02361. <https://arxiv.org/abs/1910.02361>

Kubota, K., Yoshiura, S., Takahashi, K., et al. 2018, MNRAS, 479, 2754, doi: [10.1093/mnras/sty1471](https://doi.org/10.1093/mnras/sty1471)

Mesinger, A., Furlanetto, S., & Cen, R. 2011, MNRAS, 411, 955, doi: [10.1111/j.1365-2966.2010.17731.x](https://doi.org/10.1111/j.1365-2966.2010.17731.x)

Morales, M. F., Hazelton, B., Sullivan, I., & Beardsley, A. 2012, ApJ, 752, 137, doi: [10.1088/0004-637X/752/2/137](https://doi.org/10.1088/0004-637X/752/2/137)

Neben, A. R., Stalder, B., Hewitt, J. N., & Tonry, J. L. 2017, ApJ, 849, 50, doi: [10.3847/1538-4357/aa8f9c](https://doi.org/10.3847/1538-4357/aa8f9c)

Silva, M. B., Santos, M. G., Gong, Y., Cooray, A., & Bock, J. 2013, ApJ, 763, 132, doi: [10.1088/0004-637X/763/2/132](https://doi.org/10.1088/0004-637X/763/2/132)

Silva, M. B., & Zaroubi, S. 2018, in IAU Symposium, Vol. 333, Peering towards Cosmic Dawn, ed. V. Jelić & T. van der Hulst, 250–253

Sobacchi, E., Mesinger, A., & Greig, B. 2016, MNRAS, 459, 2741, doi: [10.1093/mnras/stw811](https://doi.org/10.1093/mnras/stw811)

Appendix

This is where appendix-y things go

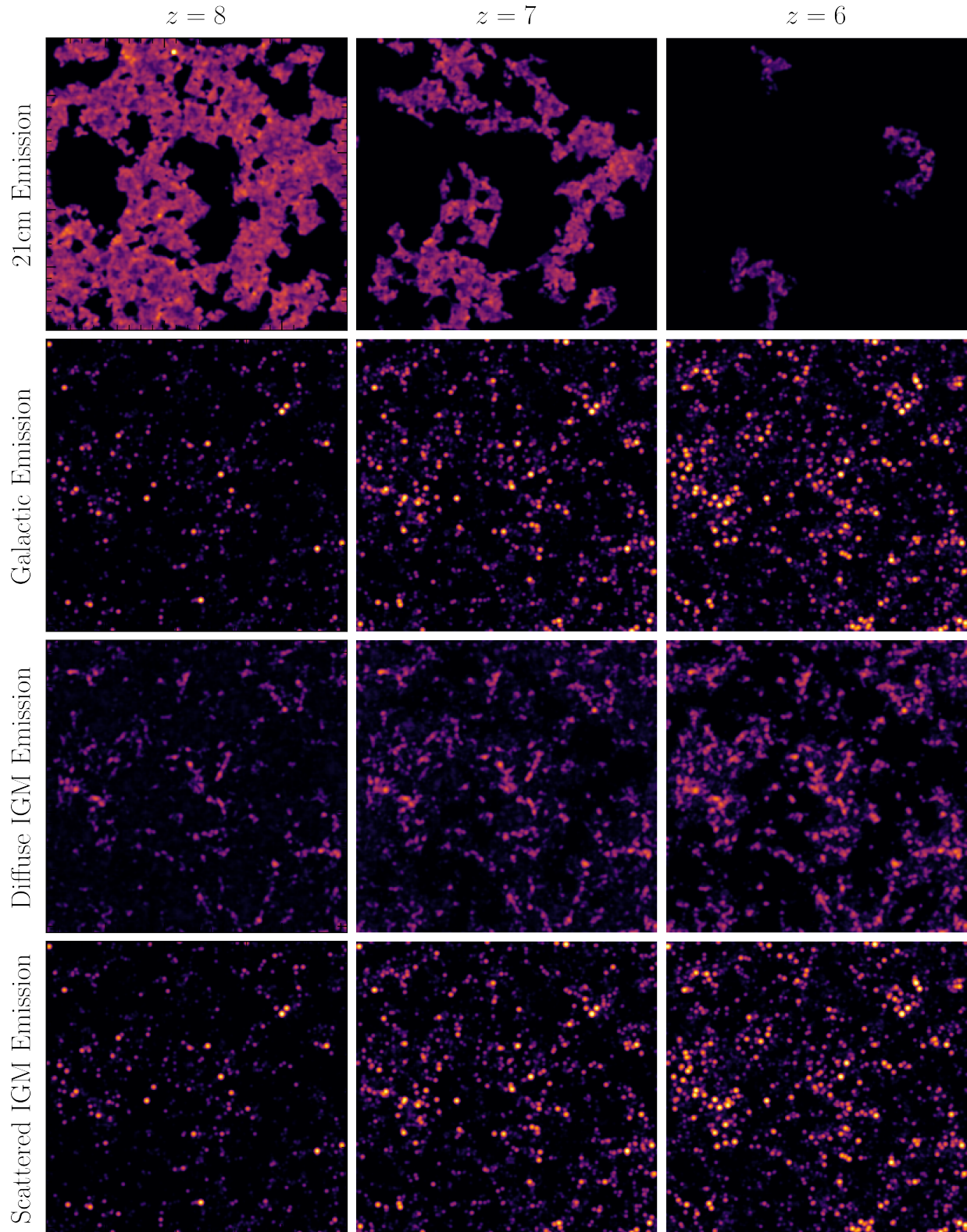
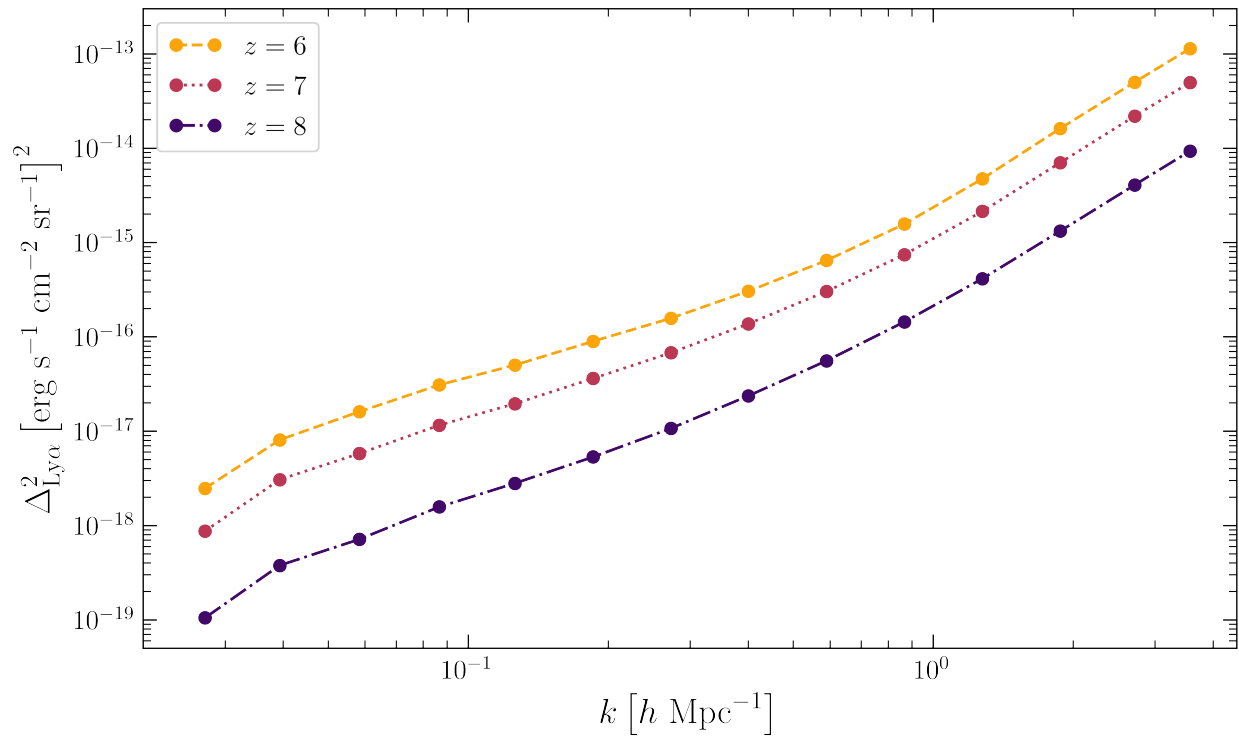
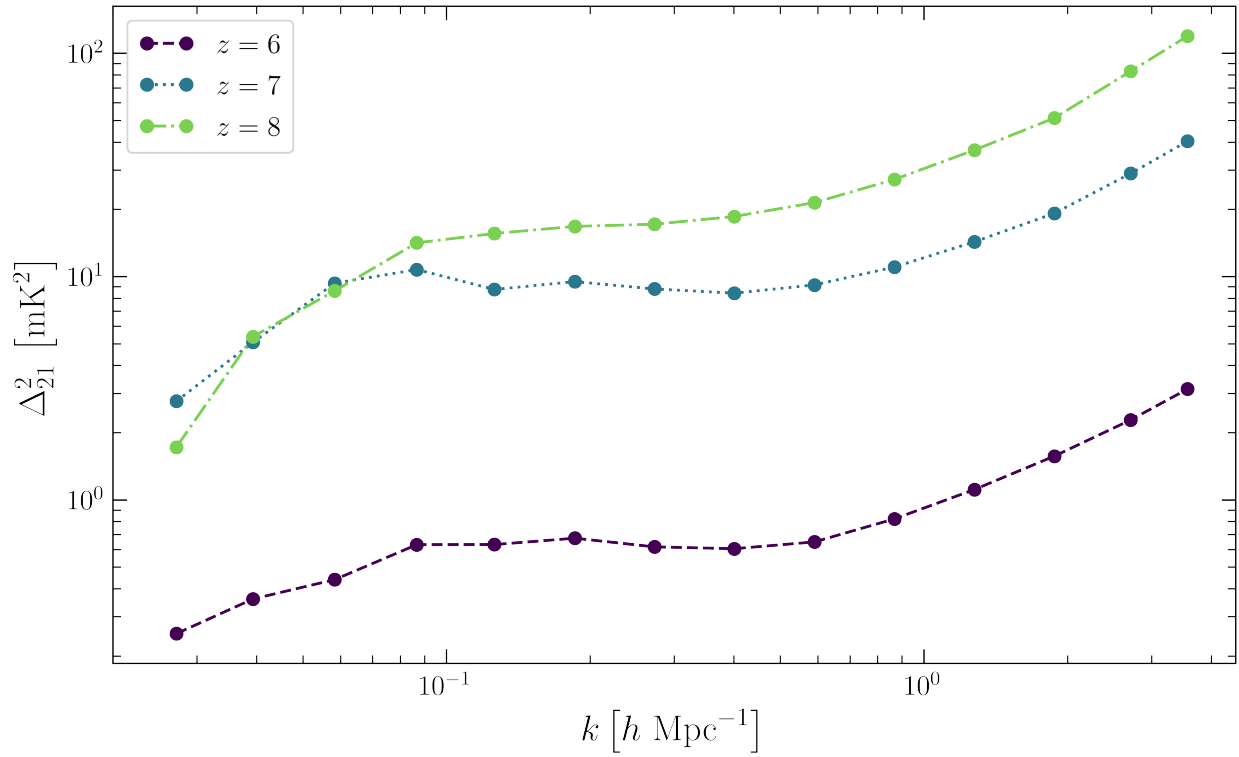


Figure 6. Simulated 21cm and Ly α emission as described in section blah. Each column represents simulated emission at different redshift value.



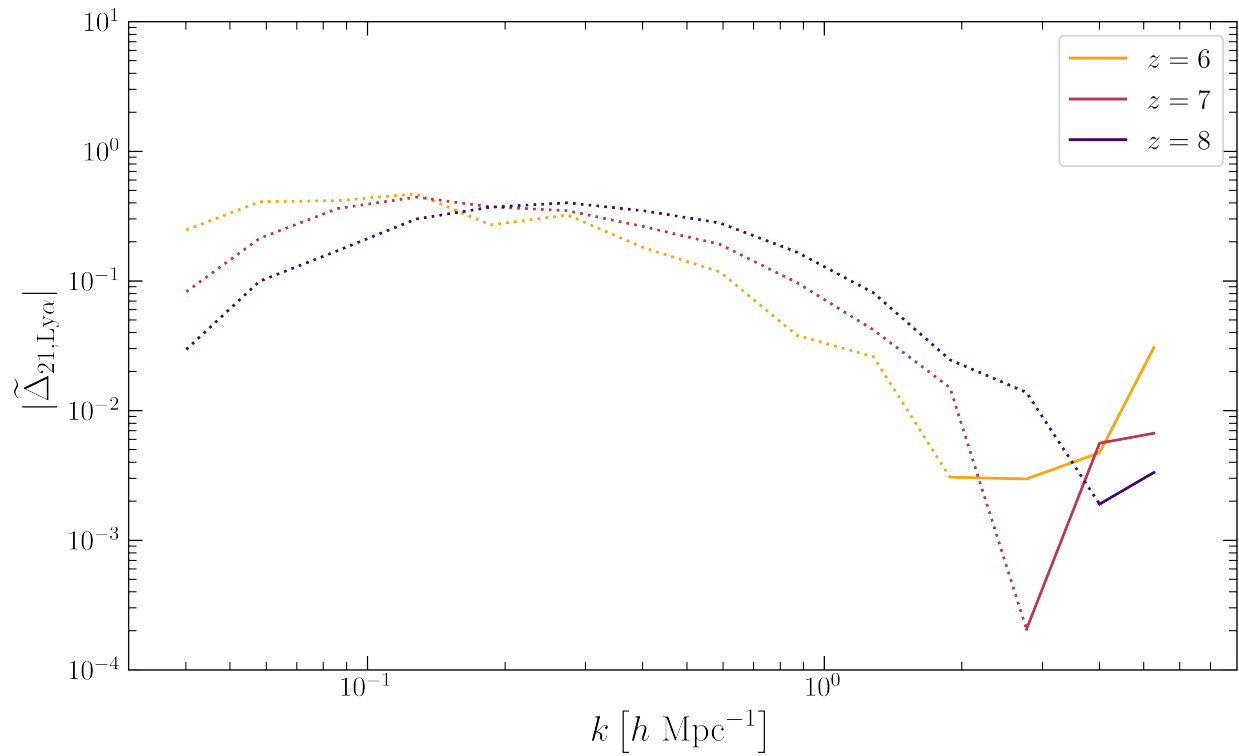


Figure 9. Cross-correlation coefficient

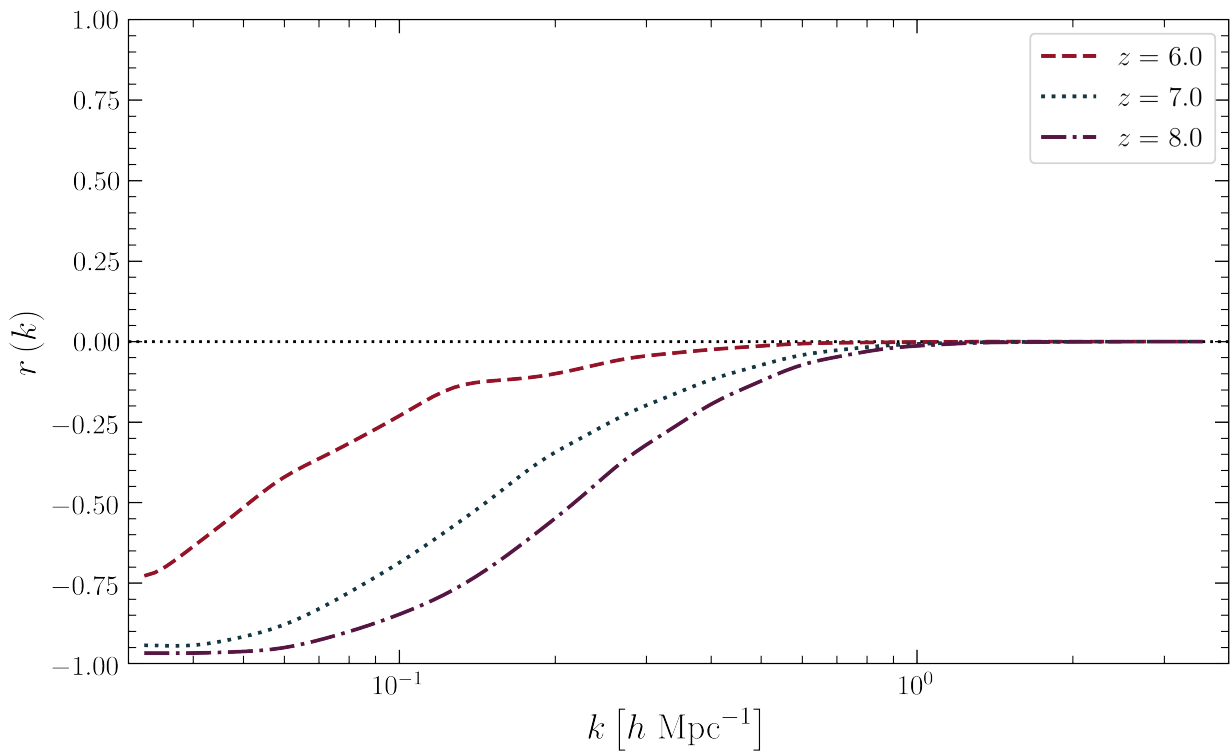


Figure 10. Cross-correlation coefficient

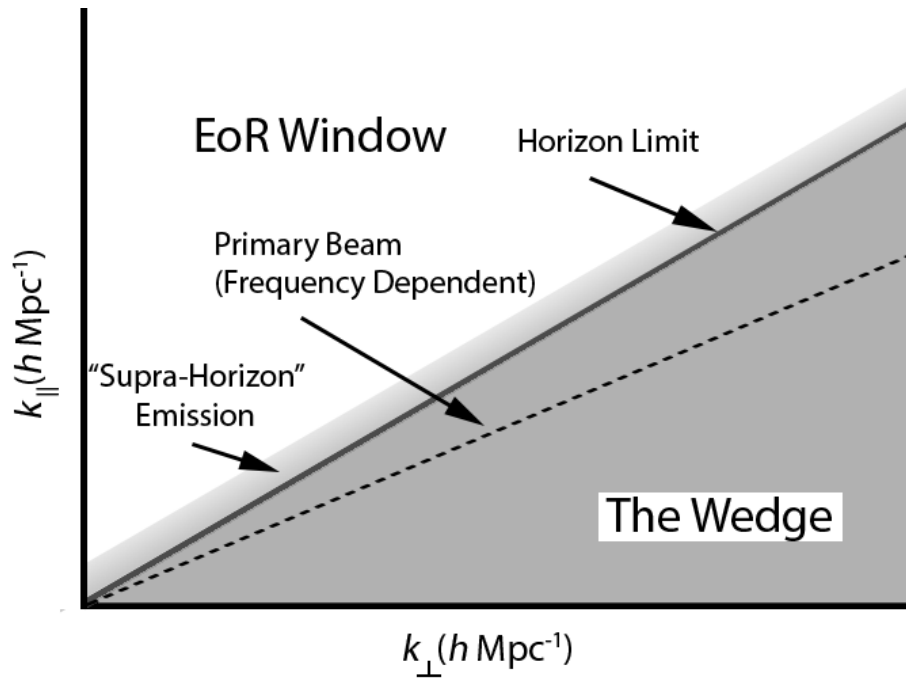


Figure 11. Foreground Wedge

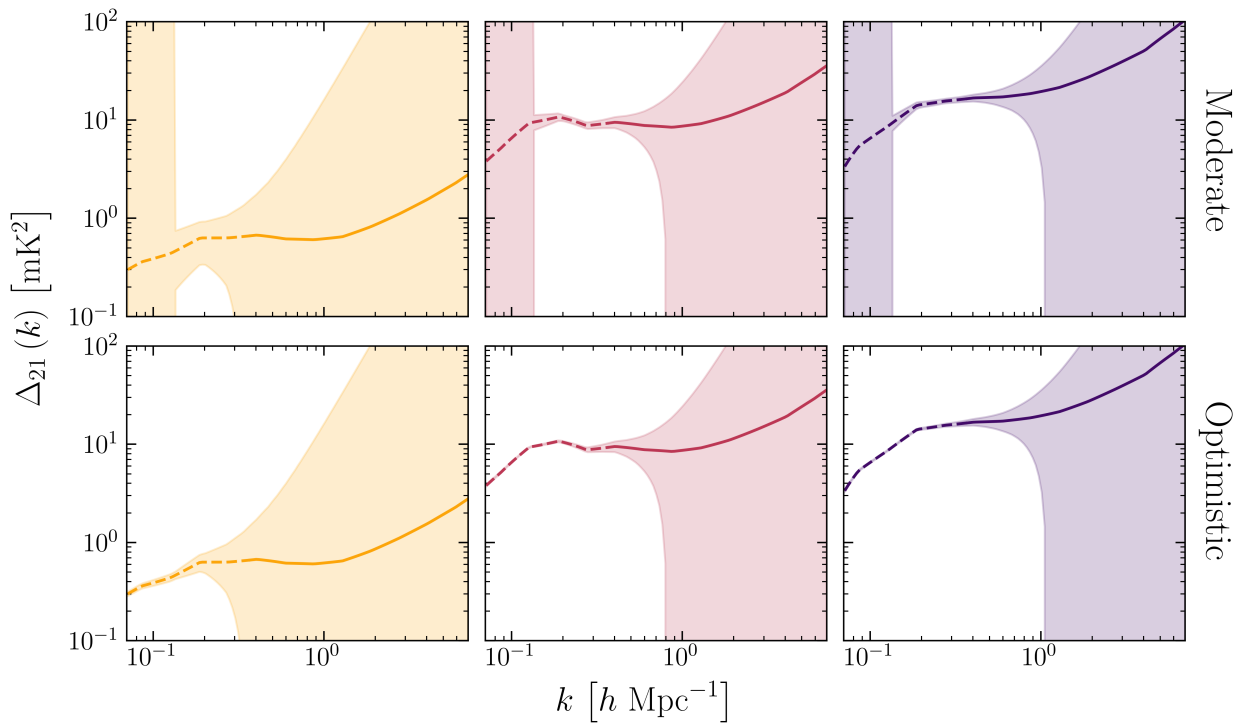


Figure 12. Hello

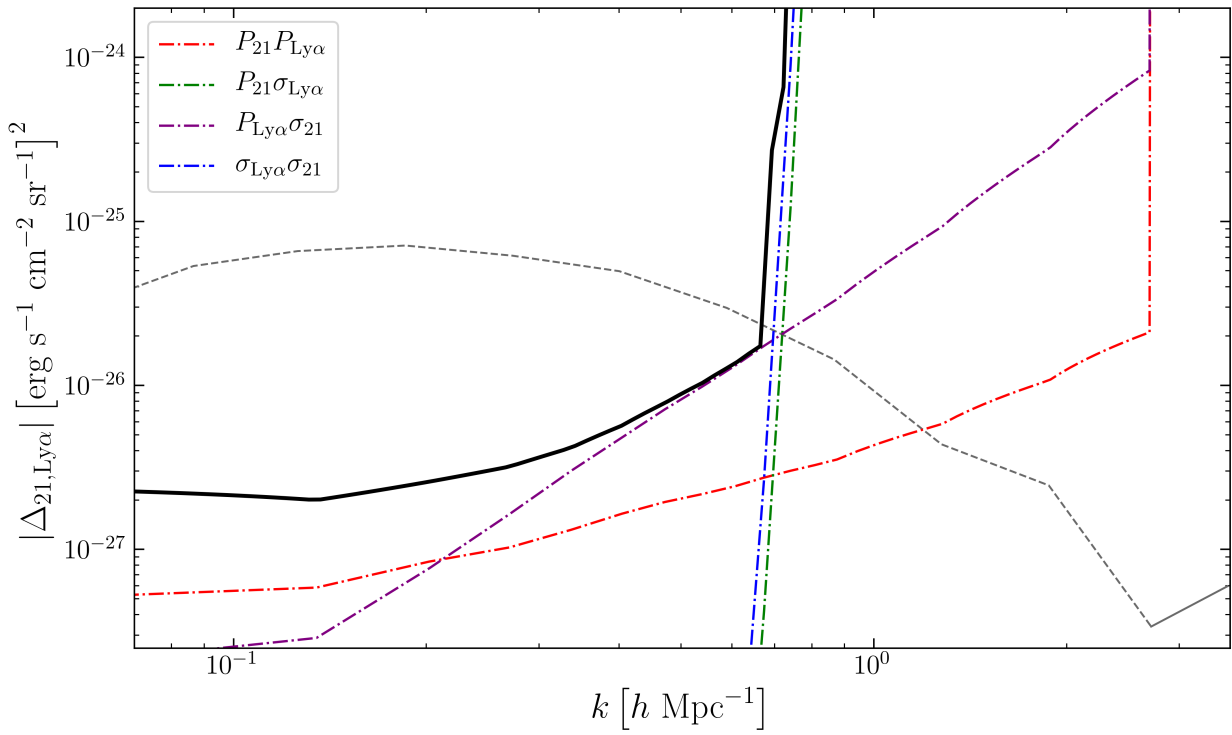


Figure 13. Hello

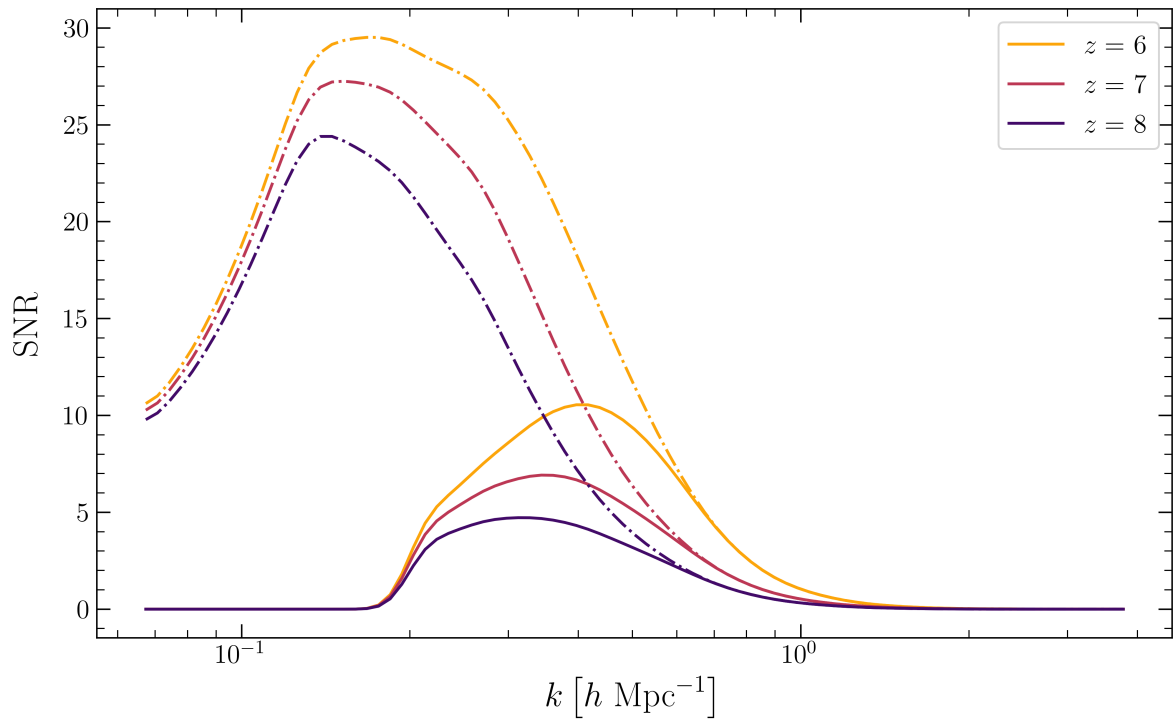


Figure 14. Hello